photonics

MDPI

Communication

Evolution of the Phase Singularity of an Orbital Angular Momentum Beam with an Astigmatism Phase

Chunhao Liang [1,2], Cuiling Zheng [1,2], Xinru Lian [1,2], Qian Chen [1,2], Yaru Gao [1,2,*], Jinsong Liu [1,2], Yangjian Cai [1,2] and Jun Zeng [1,2,*]

[1] Shandong Provincial Engineering and Technical Center of Light Manipulation & Shandong Provincial Key Laboratory of Optics and Photonics Devices, School of Physics and Electronics, Shandong Normal University, Jinan 250014, China; chunhaoliang@sdnu.edu.cn (C.L.); 2021020559@stu.sdnu.edu.cn (C.Z.); 202009100427@stu.sdnu.edu.cn (X.L.); 2020020538@stu.sdnu.edu.cn (Q.C.); liujs@sdnu.edu.cn (J.L.); yangjiancai@sdnu.edu.cn (Y.C.)

[2] Collaborative Innovation Center of Light Manipulations and Applications, Shandong Normal University, Jinan 250358, China

* Correspondence: gaoyaru@sdnu.edu.cn (Y.G.); zengjun@sdnu.edu.cn (J.Z.)

Abstract: In this study, we explore the impact of the astigmatism phase on the evolution of the phase singularity of an orbital angular momentum (OAM) beam propagating through free space. The results demonstrate that the high-order phase singularity dispersed into a cluster of individual unit phase singularities owing to the astigmatism phase. The number of singularities equaled the topological charge of the OAM beam. By adjusting the astigmatism phase, we could manipulate and control the evolution of the phase singularities, including their displacements and rotation angles. These findings offer significant prospects for customizing 3D vortex lines, optical topologies, and applications involving topological charge measurement, information encoding, and transfer.

Keywords: phase singularity; astigmatism phase; orbital angular momentum beam

Citation: Liang, C.; Zheng, C.; Lian, X.; Chen, Q.; Gao, Y.; Liu, J.; Cai, Y.; Zeng, J. Evolution of the Phase Singularity of an Orbital Angular Momentum Beam with an Astigmatism Phase. *Photonics* **2024**, *11*, 149. https://doi.org/10.3390/photonics11020149

Received: 8 January 2024
Revised: 25 January 2024
Accepted: 1 February 2024
Published: 5 February 2024

1. Introduction

Vortex beams, also known as orbital angular momentum (OAM) beams, exhibit a helical phase structure around the optical axis, resulting in a phase singularity in which the phase is undefined. This causes the energy to concentrate around this axis, creating a central dark zone in the intensity profile [1]. Over the past few decades, OAM beams have emerged as a prominent topic in the optical community. They have numerous applications in optical imaging, particle trapping, and optical communication [2–7]. Recently, significant progress has been achieved by upgrading the protocol for number factorization using OAM beams [8]. In particular, since the pioneering work of Berry [9], the optical framed topology, which is formed by the spatial evolution of the phase singularity, has garnered considerable interest [10–13] because of its vital applications in a wide range of areas, such as programmable 3D particle manipulation, topological quantum computing, and high-capacity and high-security information encoding [14–18]. In principle, the design of the topology structure strongly depends on the manipulation of the evolutionary trajectory of the phase singularities in 3D space. Most research efforts have concentrated on the manipulation of the two-dimensional phase singularity distribution at the light source or on the receiving plane [19–22]. However, there are relatively few studies on the evolution of the spatial trajectories of phase singularities, particularly in terms of flexible manipulation.

The cross-phase, which is one of the more active astigmatism phases, plays a crucial role in the manipulation and applications of light beams. For example, Liang et al. discovered a mutual conversion of modes between Laguerre–Gaussian beams and Hermite–Gaussian beams by implementing a cross-phase [23]. As a result, the detection of the topological features of Laguerre–Gaussian beams has become much simpler, only requiring the cross-phase to

be introduced into the pre-measured beams to convert them into Hermite–Gaussian profiles. The topological charge of Laguerre–Gaussian beams has a deterministic relationship with the number of side lobes in the Hermite–Gaussian profile, and this relationship is independent of the optical coherence of the beam, even at extremely low coherence levels [24]. Additionally, by utilizing the cross phase, the beam can be rotated during propagation, autofocusing can be performed flexibly, the z-coherence can be enhanced, beam polygonal shaping can be executed, and the beam scintillation of the turbulent disturbance can be mitigated [25–31]. The cross-phase provides the partially coherent beam with the ability to shape distortions that may occur owing to optical diffraction and obstacles, facilitating robust far-field optical imaging [32–34]. However, the present research efforts primarily focus on using cross-phase to manipulate electric fields, intensity, optical coherence, etc., and have not yet used it to carry out phase control of the beam itself.

In this study, we aim to flexibly control the evolution behavior of the phase singularity of an OAM beam in three dimensions with the help of the cross-phase. The rest of this paper is organized as follows: Section 2 describes the theoretical model and methods, Section 3 presents an analysis of the results, and Section 4 contains the conclusions.

2. Theoretical Model and Method

To fully explore the effect of the astigmatism phase on the OAM beam, we modeled the OAM beam as a Bessel–Gaussian beam. In polar coordinates (ρ, θ), the amplitude of the OAM beam E_0 is expressed as

$$E_0(\rho, \theta) = J_l(k_l \rho) \exp\left(-\rho^2/\omega_0^2\right) \exp(il\theta) \tag{1}$$

where J_l represents the l^{th}-order Bessel function of the first kind, k_l is a radial parameter, ω_0 is the beam width, and l is the topological charge. We also introduced the cross-phase $\exp\left(iu\rho_\perp\rho_\parallel\right)$, as the astigmatism phase into the OAM beam, where $\left(\rho_\perp, \rho_\parallel\right)$ represents the Cartesian coordinates, and u is the strength factor. The propagation properties of the beam were examined using the angular spectrum principle, which is expressed as

$$E_z(x, y) = F_T^{-1}\left\{F_T\left[E_0(\rho, \theta)\exp\left(iu\rho_\perp\rho_\parallel\right)\right] \times \exp\left[ikz\sqrt{1-(\lambda\xi_\perp)^2-\left(\lambda\xi_\parallel\right)^2}\right]\right\} \tag{2}$$

where $\left(\xi_\perp, \xi_\parallel\right)$ and (x, y) denote the positions in the Fourier and receiver planes, respectively, $k = 2\pi/\lambda$ is the wavenumber, λ is the wavelength, and F_T represents the Fourier transform.

To locate the phase singularities, we adopted the protocol proposed by Fried [35,36]. This protocol involved connecting the phase singularities at various propagation distances, which allowed us to derive the evolution of the spatial trajectories of the singularities. To characterize the singularity of a point, we used a path integral along the closed loop surrounding it [35,36], which can be expressed as

$$m = \frac{1}{2\pi}\oint_C \nabla\varphi(\mathbf{r})d\mathbf{r} \tag{3}$$

where m is the topological charge of the singularity, C is a tiny closed loop surrounding the singularity, ∇ represents the Laplacian operator, and $\varphi(\mathbf{r})$ is the phase of the electric field $E_z(x, y)$. Following the details described in [35,36], the integrand in Equation (3) can be rewritten in discrete form as

$$\begin{aligned}\nabla\varphi(\mathbf{r}) = \nabla\varphi[id, jd] = {} & \tfrac{1}{d}\tan^{-1}\left\{\frac{\mathrm{Im}[E_z[(i+1)d,jd]E_z^*(id,jd)]}{\mathrm{Re}[E_z[(i+1)d,jd]E_z^*(id,jd)]}\right\}\hat{x} \\ & + \tfrac{1}{d}\tan^{-1}\left\{\frac{\mathrm{Im}[E_z[id,(j+1)d]E_z^*(id,jd)]}{\mathrm{Re}[E_z[id,(j+1)d]E_z^*(id,jd)]}\right\}\hat{y}\end{aligned} \tag{4}$$

where the electric field E_z in the receiver plane was represented as a matrix with N × N elements (N represents the number of sampling points along both the horizontal and vertical directions) and was assumed to have the physical dimensions of L × L (L represents the length of the coordinate); d = L/N is the sampling interval; i and j represent the sequence number of the points in the horizontal and vertical directions (which ranged within the interval [1, N − 1]), respectively; Im and Re represent the imaginary and real parts of the function, respectively; and $\hat{x}$ and $\hat{y}$ are the unit vectors in the x- and y-directions, respectively.

We defined the integral contours in Equation (3) as a 2 × 2-pixel array, which can be rewritten in discrete form as

$$S_{ij} = \frac{d}{2\pi}\{\nabla\varphi[id, jd]\hat{x} + \nabla\varphi[(i+1)d, jd]\hat{y} - \nabla\varphi[id, (j+1)d]\hat{x} - \nabla\varphi[id, jd]\hat{y}\} \quad (5)$$

If a phase singularity was enclosed, then S_{ij} was equal to the topological charge m. We evaluate Equations (4) and (5) globally to ensure that all phase singularities across the entire beam section are determined.

3. Numerical Results and Analysis

Using the optical wave propagation method and the equations listed above, we explored the impact of the cross-phase on the evolution of the phase singularities of an OAM beam as it propagated through free space. The relevant parameters were as follows: $k_l = 10\ \mathrm{mm}^{-1}$, $\omega_0 = 1$ mm, L = 8 mm, and N = 2048. Specific explanations of the other parameters are provided below.

Figure 1 displays the phase evolution of Bessel–Gaussian beams propagating through free space without (top row) and with (bottom row) the cross-phase. The phase distributions of the pure Bessel–Gaussian beam in the source plane and the cross-phase are presented in the first column. In the absence of the cross-phase, the phase distributions of the Bessel–Gaussian beam were twisted because of the spherical wave as it propagated. However, the high-order phase singularity (indicated by the red dots) remained intact and did not shift. In the presence of the cross-phase, the phase singularity of the Bessel–Gaussian beam was unstable and split into two unit phase singularities. The number of unit phase singularities was equal to the topological charge. This observation provided a simple protocol for measuring the topological charge of the OAM beam, in which the presence of phase singularities resulted in null-intensity regions, allowing the topological charge to be determined by counting the number of null-intensity cores across the intensity profile. Furthermore, as the beam propagated, the phase singularities not only moved apart but also underwent rotational motion in space. Subsequently, to fully understand the influence of the cross-phase on the dynamics of the phase singularities, we specifically concentrated on the phase singularities rather than on analyzing the overall phase distributions.

Next, we adopted the method described above to locate the phase singularities and study the evolution of the singularities in the OAM beam during propagation. In Figure 2, we show the evolution of the spatial trajectories of the phase singularities of the OAM beams with different topological charges. The results demonstrate the high-order phase singularities tended to split into a cluster of individual unit phase singularities (here, the curves characterize the unit phase singularity) owing to the presence of the cross-phase. Curves with the same color but different line types represent different phase singularities originating from the same OAM source, and different colors represent the OAM beams with different topological charges. One found that the number of curves (representing the unit phase singularities) was equal to the topological charge. Moreover, the distributions of the phase singularities exhibited a symmetric pattern around the origin. As the propagation distance increased, these singularities gradually drifted away from the origin, as shown in the left-hand panel of Figure 2. To provide a clearer visualization of the evolution of the singularities, the right-hand panel in Figure 2 presents a top view of the distribution. Figure 3 shows the effect of the strength factor of the cross-phase on the evolution of the phase singularities of the OAM beam. Because of the topological charge l = 2, the high-order

phase singularity splits into two unit phase singularities (resulting in two curves). The left-hand panel presents the trajectories in three dimensions, and the right-hand panel displays the top view. The figure clearly demonstrates that the displacements and rotation angles of the phase singularities changed as the beam propagated and that these changes depended on the strength factor of the cross-phase. This indicates the potential for manipulating and controlling the behavior of phase singularities by adjusting the cross-phase.

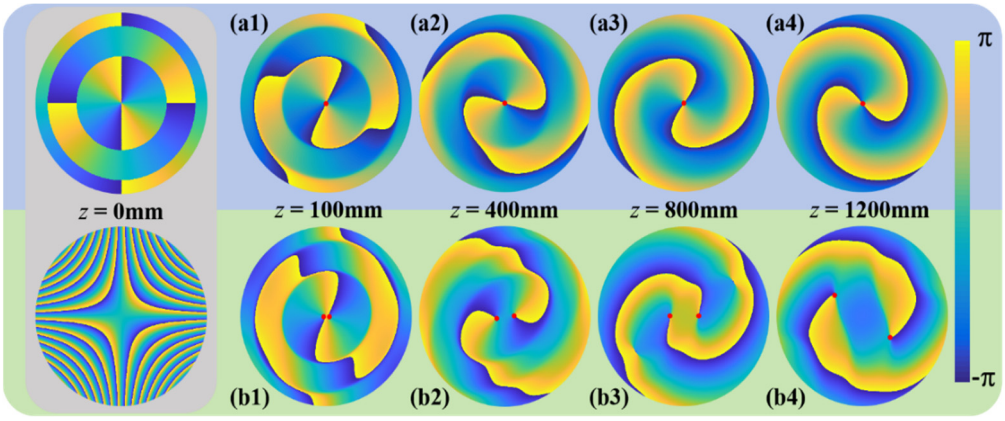

Figure 1. Phase evolution of Bessel–Gaussian beams propagating through free space without (**a1**–**a4**) and with (**b1**–**b4**) the cross-phase. The phase distributions of the pure Bessel–Gaussian beam and the cross-phase are shown at the bottom and top, respectively, of the first column. The red dots denote the phase singularities. The topological charge was $l = 2$.

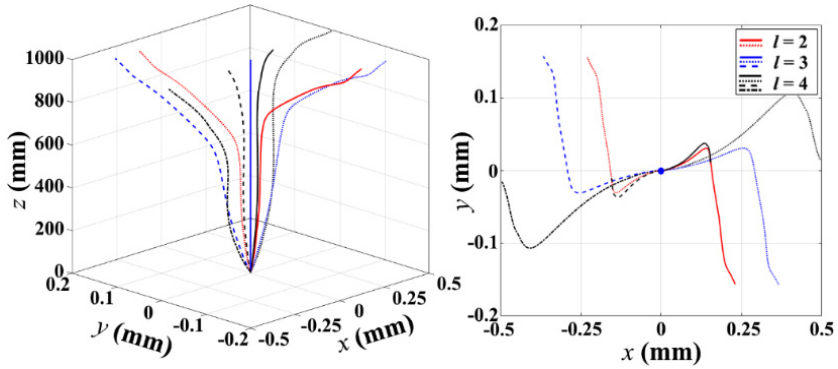

Figure 2. Evolution of the phase singularities of the OAM beam with different topological charges during propagation. The cross-phase strength factor was $u = 6$ mm^{-2}. Curves with the same color but different line types represent different phase singularities originating from the same OAM source.

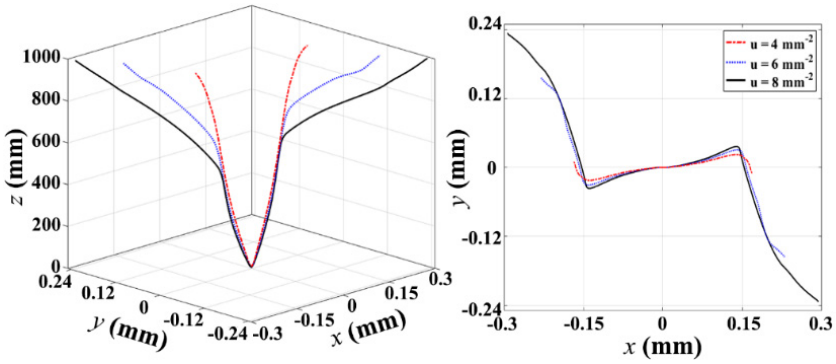

Figure 3. Evolution of the phase singularities of the OAM beam with different strength factors during propagation. The topological charge was $l = 2$.

To describe the evolution of the phase singularity quantitatively, we defined the displacement and rotation angle of the phase singularity $P_j(x, y, z)$ as $\Delta d = \sqrt{x^2 + y^2}$ and $\theta_{\text{rot}} = \arctan(y/x)$, respectively. Because of the symmetric distribution of the evolutionary trajectory of the phase singularity around the origin, we focused solely on the phase singularities located in the right half of the right-hand panels shown in Figures 2 and 3. In Figure 4, the displacements and rotation angles of the phase singularities of the OAM beam are plotted in the left-hand and right-hand panels, respectively. The strength factor was u = 6 mm^{-2}. The displacement of the phase singularity increased steadily as the propagation distance increased. For l = 3, the central phase singularity propagated along the optical axis and remained stable without deflections. This observation can serve as a reference point and potentially facilitate information detection. The displacement of the outermost phase singularity increased as the topological charge increased. For the rotation angles, the phase singularities were first rotated counterclockwise and then clockwise. The smaller the topological charge, the smaller the propagation distance corresponding to a given change in the rotation direction. Although the displacements of different phase singularities from the same OAM beam (see the black solid and dotted curves in Figure 4) varied significantly, their rotation angle trends were nearly identical. Furthermore, we assumed l = 2 and quantitatively examined the effect of the cross-phase on the evolution of the phase singularities. The left-hand and right-hand panels in Figure 5 show the results for the displacements and rotation angles, respectively. The figure demonstrates that as the strength factor increased, the displacement increased, and the angular velocity in the counterclockwise and clockwise directions also increased. Furthermore, the propagation distance corresponding to a given change in the rotation direction decreased as the strength factor increased. This suggests that a larger strength factor enhances the phase singularity. The unexpected fluctuations in the curves shown in the two figures above were primarily due to undersampling (i.e., the sampling interval was not sufficiently small to adequately smooth the curves).

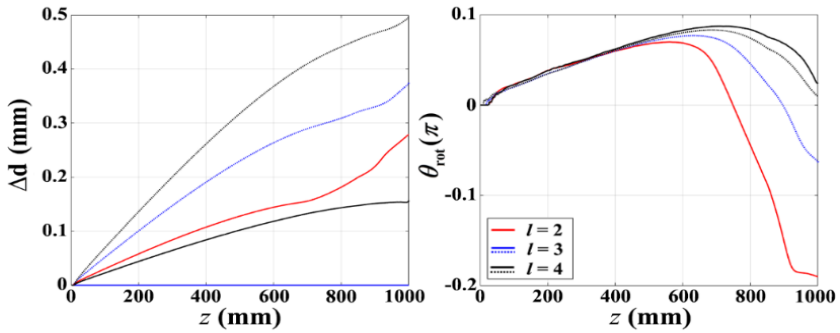

Figure 4. Evolution of displacements and rotation angles of the phase singularities of the OAM beam with different topological charges during propagation. The strength factor was u = 6 mm^{-2}. Curves with the same color but different line types represent different phase singularities originating from the same OAM source.

Finally, we studied the evolution of the displacements and rotation angles of the phase singularities of the OAM beam as a function of the strength factor for a propagation distance of z = 1000 mm. The results are displayed in Figure 6. When u = 0 mm^{-2} (i.e., without the cross-phase), the displacement was equal to 0, which indicates that the high-order phase singularity itself did not split. This finding is also shown in Figure 1. However, the high-order phase singularity was sensitive to external perturbations (referred to as the cross-phase in this study); thus, it was split into a cluster of individual unit phase singularities. As expected, when the strength factor increased, the displacements of the singularities increased (as shown in the left-hand panel in Figure 6). The right-hand panel in Figure 6 shows that the strength factor strongly influenced the rotation direction and angle. These results demonstrate that the displacement and rotation angle have a deterministic

relationship with the strength factor. Therefore, the evolution of the spatial trajectory of the phase singularity can be fully determined by manipulating the cross-phase.

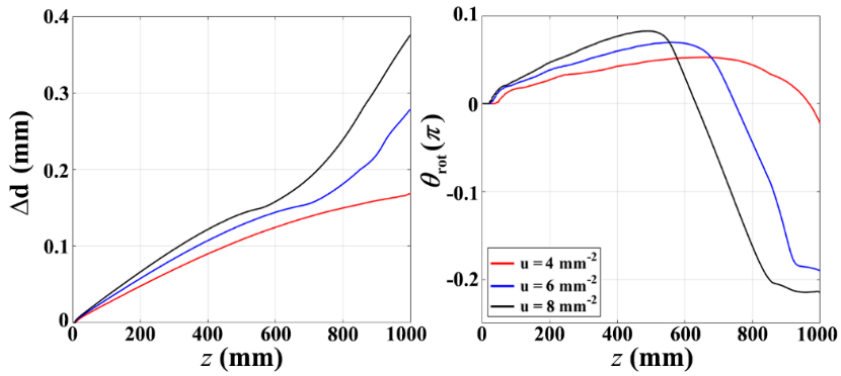

Figure 5. Evolution of displacements and rotation angles of the phase singularities of the OAM beam with different strength factors during propagation. The topological charge was $l = 2$.

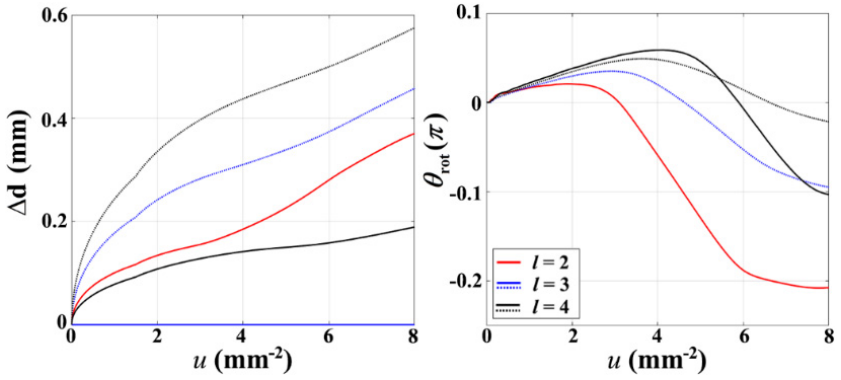

Figure 6. Evolution of displacements and rotation angles of the phase singularities of the OAM beam with different topological charges as a function of the strength factor for a propagation distance of z = 1000 mm.

4. Conclusions

In this study, we investigated the effect of the cross-phase, as the astigmatism phase, on the evolution of the phase singularity in an OAM beam. We found that the high-order phase singularity was unstable and split into a group of unit phase singularities because of the presence of the cross-phase. The number of phase singularity curves was equal to the topological charge, and the phase singularities contributed to null-intensity cores. Hence, by counting the null-intensity cores across the intensity profile, the topological charge of the OAM beam could be determined. By exploiting the cross-phase, we were able to flexibly manipulate and control the evolution of phase singularities, including their displacements and rotation angles. The results achieved in this study offer a path for achieving tunable optical topologies and provide new insights into potential applications, such as information encoding and transporting particles in programmable 3D paths.

Author Contributions: Conceptualization, C.L. and C.Z.; methodology, C.Z. and Q.C.; software, X.L.; validation, Y.C.; formal analysis, J.L.; investigation, Y.G.; data curation, C.L. and J.Z.; writing—original draft preparation, C.L.; writing—review and editing, J.L.; supervision, Y.G. and J.Z.; project administration, Y.C.; funding acquisition, C.L., Y.C. and J.Z. All authors have read and agreed to the published version of the manuscript.

Funding: The National Key Research and Development Program of China (Grant Nos. 2022YFA1404800 and 2019YFA0705000), the National Natural Science Foundation of China (Grant Nos. 12374311, 11974218, 12104264 and 92250304), the Qingchuang Science and Technology Plan of Shandong Province

(Grant No. 2022KJ246), the China Postdoctoral Science Foundation (Grant No. 2022T150392), and the Natural Science Foundation of Shandong Province (Grant No. ZR2023YQ006 and ZR2021QA014).

Institutional Review Board Statement: Not applicable.

Informed Consent Statement: Not applicable.

Data Availability Statement: Data underlying the results presented in this paper are not publicly available at this time but may be obtained from the authors upon reasonable request.

Conflicts of Interest: The authors declare no conflicts of interest.

References

1. Coullet, P.; Gil, L.; Rocca, F. Optical Vortices. *Opt. Commun.* **1989**, *73*, 403–408. [CrossRef]
2. Ashkin, A. Acceleration and Trapping of Particles by Radiation Pressure. *Phys. Rev. Lett.* **1970**, *24*, 156–159. [CrossRef]
3. Wang, J.; Yang, J.-Y.; Fazal, I.M.; Ahmed, N.; Yan, Y.; Huang, H.; Ren, Y.; Yue, Y.; Dolinar, S.; Tur, M.; et al. Terabit Free-Space Data Transmission Employing Orbital Angular Momentum Multiplexing. *Nat. Photonics* **2012**, *6*, 488–496. [CrossRef]
4. Lavery, M.P.J.; Robertson, D.J.; Berkhout, G.C.G.; Love, G.D.; Padgett, M.J.; Courtial, J. Refractive Elements for the Measurement of the Orbital Angular Momentum of a Single Photon. *Opt. Express* **2012**, *20*, 2110–2115. [CrossRef] [PubMed]
5. Padgett, M.; Bowman, R. Tweezers with a Twist. *Nat. Photonics* **2011**, *5*, 343–348. [CrossRef]
6. Yang, Y.; Ren, Y.; Chen, M.; Arita, Y.; Rosales-Guzmán, C. Optical Trapping with Structured Light: A Review. *Adv. Photonics* **2021**, *3*, 034001. [CrossRef]
7. Xie, X.; Chen, Y.; Yang, K.; Zhou, J. Harnessing the Point-Spread Function for High-Resolution Far-Field Optical Microscopy. *Phys. Rev. Lett.* **2014**, *113*, 263901. [CrossRef] [PubMed]
8. Li, X.; Liu, X.; Wu, Q.; Zeng, J.; Cai, Y.; Sergey, A.; Ponomarekno; Liang, C. Prime Number Factorization with Light Beams Carrying Orbital Angular Momentum. *submitted*.
9. Berry, M.V.; Dennis, M.R. Knotted and Linked Phase Singularities in Monochromatic Waves. *Proc. R. Soc. Lond. Ser. A Math. Phys. Eng. Sci.* **2001**, *457*, 2251–2263. [CrossRef]
10. Pisanty, E.; Machado, G.J.; Vicuña-Hernández, V.; Picón, A.; Celi, A.; Torres, J.P.; Lewenstein, M. Knotting Fractional-Order Knots with the Polarization State of Light. *Nat. Photonics* **2019**, *13*, 569–574. [CrossRef]
11. Wang, L.; Zhang, W.; Yin, H.; Zhang, X. Ultrasmall Optical Vortex Knots Generated by Spin-Selective Metasurface Holograms. *Adv. Opt. Mater.* **2019**, *7*, 1900263. [CrossRef]
12. Dennis, M.R.; King, R.P.; Jack, B.; O'Holleran, K.; Padgett, M.J. Isolated Optical Vortex Knots. *Nat. Phys.* **2010**, *6*, 118–121. [CrossRef]
13. Leach, J.; Dennis, M.R.; Courtial, J.; Padgett, M.J. Vortex Knots in Light. *New J. Phys.* **2005**, *7*, 55. [CrossRef]
14. Rodrigo, J.A.; Angulo, M.; Alieva, T. Programmable Optical Transport of Particles in Knot Circuits and Networks. *Opt. Lett.* **2018**, *43*, 4244–4247. [CrossRef]
15. Romero, J.; Leach, J.; Jack, B.; Dennis, M.R.; Franke-Arnold, S.; Barnett, S.M.; Padgett, M.J. Entangled Optical Vortex Links. *Phys. Rev. Lett.* **2011**, *106*, 100407. [CrossRef] [PubMed]
16. Larocque, H.; D'Errico, A.; Ferrer-Garcia, M.F.; Carmi, A.; Cohen, E.; Karimi, E. Optical Framed Knots as Information Carriers. *Nat. Commun.* **2020**, *11*, 5119. [CrossRef]
17. Kong, L.-J.; Zhang, W.; Li, P.; Guo, X.; Zhang, J.; Zhang, F.; Zhao, J.; Zhang, X. High Capacity Topological Coding Based on Nested Vortex Knots and Links. *Nat. Commun.* **2022**, *13*, 2705. [CrossRef]
18. Zhu, J.; Zhang, H.; Wang, Z.; Zhao, X.; Lu, X.; Cai, Y.; Zhao, C. Coherence Singularity and Evolution of Partially Coherent Bessel–Gaussian Vortex Beams. *Opt. Express* **2023**, *31*, 9308–9318. [CrossRef] [PubMed]
19. Wang, Y.; Ma, H.; Tai, Y.; Li, X. Generation of Discrete Higher-Order Optical Vortex Lattice at Focus. *Opt. Lett.* **2023**, *48*, 4464–4467. [CrossRef]
20. Zhu, L.; Tai, Y.; Li, H.; Hu, H.; Li, X.; Cai, Y.; Shen, Y. Multidimensional Optical Tweezers Synthetized by Rigid-Body Emulated Structured Light. *Photonics Res.* **2023**, *11*, 1524–1534. [CrossRef]
21. Piccardo, M.; de Oliveira, M.; Toma, A.; Aglieri, V.; Forbes, A.; Ambrosio, A. Vortex Laser Arrays with Topological Charge Control and Self-Healing of Defects. *Nat. Photonics* **2022**, *16*, 359–365. [CrossRef]
22. Singh, R.K.; Sharma, A.M.; Senthilkumaran, P. Vortex Array Embedded in a Partially Coherent Beam. *Opt. Lett.* **2015**, *40*, 2751–2754. [CrossRef] [PubMed]
23. Liang, G.; Wang, Q. Controllable Conversion between Hermite Gaussian and Laguerre Gaussian Modes Due to Cross Phase. *Opt. Express* **2019**, *27*, 10684–10691. [CrossRef] [PubMed]
24. Zhang, Z.; Liu, Z.; Liu, X.; Gbur, G.; Liang, C.; Cai, Y.; Zeng, J. Measuring the Orbital Angular Momentum of a Vortex Beam under Extremely Low Coherence. *Appl. Phys. Lett.* **2023**, *122*, 011101. [CrossRef]
25. Shen, D.; Zhao, D. Measuring the Topological Charge of Optical Vortices with a Twisting Phase. *Opt. Lett.* **2019**, *44*, 2334–2337. [CrossRef] [PubMed]
26. Wang, C.; Ren, Y.; Liu, T.; Luo, C.; Qiu, S.; Li, Z.; Wu, H. Generation and Measurement of High-Order Optical Vortices by Using the Cross Phase. *Appl. Opt.* **2020**, *59*, 4040–4047. [CrossRef] [PubMed]

27. Ren, Y.; Wang, C.; Liu, T.; Wang, Z.; Yin, C.; Qiu, S.; Li, Z.; Wu, H. Polygonal Shaping and Multi-Singularity Manipulation of Optical Vortices Via High-Order Cross-Phase. *Opt. Express* **2020**, *28*, 26257–26266. [CrossRef]
28. Wan, L.; Zhao, D. Controllable Rotating Gaussian Schell-Model Beams. *Opt. Lett.* **2019**, *44*, 735–738. [CrossRef] [PubMed]
29. Xin, L.; Li, Z.; Monfared, Y.E.; Liang, C.; Wang, F.; Hoenders, B.J.; Cai, Y.; Ma, P. Flexible Autofocusing Properties of Ring Pearcey Beams by Means of a Cross Phase. *Opt. Lett.* **2021**, *46*, 70–73. [CrossRef]
30. Chang, H.; Cai, X.; Wang, F.; Zhang, Y.; Gbur, G.; Cai, Y.; Yu, J. On Z-Coherence of Schell-Model Sources Carrying a Prescribed Astigmatic Phase. *Opt. Lett.* **2023**, *48*, 558–561. [CrossRef]
31. Zhang, H.; Zhao, L.; Gao, Y.; Cai, Y.; Yuan, Y. Scintillation Mitigation Via the Cross Phase of the Gaussian Schell-Model Beam in a Turbulent Atmosphere. *Opt. Express* **2023**, *31*, 30615–30626. [CrossRef]
32. Pan, R.; Liu, X.; Tang, J.; Ye, H.; Liu, Z.; Ma, P.; Wen, W.; Hoenders, B.J.; Cai, Y.; Liang, C. Enhancing the Self-Reconstruction Ability of the Degree of Coherence of a Light Beam Via Manipulating the Cross-Phase Structure. *Appl. Phys. Lett.* **2021**, *119*, 111105. [CrossRef]
33. Liu, Y.; Chen, Y.; Wang, F.; Cai, Y.; Liang, C.; Korotkova, O. Robust Far-Field Imaging by Spatial Coherence Engineering. *Opto-Electron. Adv.* **2021**, *4*, 210027. [CrossRef]
34. Liu, Y.; Zhang, X.; Dong, Z.; Peng, D.; Chen, Y.; Wang, F.; Cai, Y. Robust Far-Field Optical Image Transmission with Structured Random Light Beams. *Phys. Rev. Appl.* **2022**, *17*, 024043. [CrossRef]
35. Fried, D.L. Branch Point Problem in Adaptive Optics. *J. Opt. Soc. Am. A* **1998**, *15*, 2759–2768. [CrossRef]
36. Ge, X.-L.; Wang, B.-Y.; Guo, C.-S. Evolution of Phase Singularities of Vortex Beams Propagating in Atmospheric Turbulence. *J. Opt. Soc. Am. A* **2015**, *32*, 837–842. [CrossRef] [PubMed]